MSSM at future Higgs factories*

Honglei Li(李洪蕾)[1][†]   Huayang Song(宋华阳)[2][‡]   Shufang Su(苏淑芳)[2][§]

Wei Su(苏伟)[3][ǂ]   Jin Min Yang(杨金民)[4,5][♯]

[1]School of Physics and Technology, University of Jinan, Jinan, Shandong 250022, China
[2]Department of Physics, University of Arizona, Tucson, Arizona 85721, USA
[3]ARC Centre of Excellence for Dark Matter Particle Physics and CSSM, Department of Physics, University of Adelaide, SA 5005, Australia
[4]CAS Key Laboratory of Theoretical Physics, Institute of Theoretical Physics, Chinese Academy of Sciences, Beijing 100190, China
[5]School of Physical Sciences, University of Chinese Academy of Sciences, Beijing 100049, China

Abstract: In this work, we study the implications of Higgs precision measurements at future Higgs factories for the MSSM parameter space, focusing on the dominant stop sector contributions. We perform a multi-variable fit to both the signal strength for various Higgs decay channels at Higgs factories and the Higgs mass. The χ^2 fit results show sensitivity to m_A, $\tan\beta$, stop mass parameter m_{SUSY}, and the stop left-right mixing parameter Xt. We also study the impact of the Higgs mass prediction on the MSSM and compare the sensitivities of different Higgs factories.

I. INTRODUCTION

After the discovery of a 125 GeV SM-like boson at the LHC [1,2], several proposals for a Higgs factory have been considered for precise measurements of the Higgs mass and couplings, including the Circular Electron Positron Collider (CEPC) in China [3], the electron-positron stage of the Future Circular Collider (FCC-ee) at CERN [4,5], and the International Linear Collider (ILC) in Japan [6]. With about 10^6 Higgs produced, the Higgs mass can be measured to an accuracy of about 10 MeV. Various Higgs couplings to the Standard Model (SM) particles can be measured at about 1% level, while the hZZ coupling can be measured at about 0.2%. If no deviation from the SM predictions is observed at future Higgs factories, severe constraints can be imposed on the parameter space of new physics models. On the other hand, if certain deviations are observed, it will provide great insights into new physics models beyond the SM, in partic-

ular, on the masses and couplings of new particles, which can be cross checked with direct searches for new particles at future high energy colliders.

In this work we focus on the implications of Higgs precision measurements for the Minimal Supersymmetric Standard Model (MSSM), which is one of the well-motivated new physics models proposed to solve the hierarchy problem [7,8]. The Higgs sector of the MSSM is the same as that of the Type-II two Higgs doublet model (2HDM), with one Higgs doublet H_u coupling to up type quarks, and the other Higgs doublet H_d coupling to down type quarks and charged leptons. After electroweak symmetry breaking, there are five physical Higgses: two *CP*-even Higgses h and H, one *CP*-odd Higgs A and a pair of charged ones $H^\pm$. In our analyses below, we take the light *CP*-even Higgs h to be the observed 125 GeV SM-like Higgs. The other possibility of the heavy *CP*-even Higgs H being the 125 GeV Higgs is tightly constrained by the

existing experimental searches, as shown in Ref. [9]. At tree level, the masses of MSSM Higgses are completely determined by only two parameters: the *CP*-odd Higgs mass m_A and the ratio of two Higgs vacuum expectation values $\tan\beta$. The mass of the SM-like light *CP*-even Higgs, however, receives large radiative corrections, with the dominant contribution from the supersymmetric top partners. The Higgs couplings to the SM sector also receive radiative corrections, characterised by the effective mixing angle α_{eff}. In addition, the bottom Yukawa coupling receives large vertex corrections. Furthermore, Higgs couplings to a pair of photons or gluons receive loop contributions from the stop sector, which are at about the same order as the SM contributions.

While in general there are more than 100 parameters in the MSSM, when we focus on the Higgs sector and the dominant loop contributions from the stop sector, only four are the most relevant: $\tan\beta$, m_A, the soft supersymmetry (SUSY) breaking stop mass parameter m_{SUSY}[1], and the left-right stop mixing parameter X_t. Other parameters, such as the mass parameters for the sbottom and gluinos, could enter as well. Those effects become important in a particular corner of the parameter space, which is left for future dedicated studies.

To study the implications of Higgs precision measurements for the parameter space of the MSSM, we perform a multi-variable χ^2 fit to both the signal strength μ for various Higgs decay channels and the Higgs mass. Earlier works on the implications of Higgs precision measurements mostly focused on the loop-induced channels $h \to gg$ and $h \to \gamma\gamma$ [10-13], given that both the SM and the MSSM contributions enter at the same order. In our work, we include all the Higgs decay channels measured at Higgs factories, as well as the Higgs mass. The MSSM predictions of those quantities have been studied extensively in the literature [14-16]. For the MSSM corrections to the Higgs couplings to the SM particles, we adopt the α_{eff} method [14,17]. We also include the additional vertex corrections to the bottom Yukawa and loop-induced couplings of hgg and $h\gamma\gamma$. We use the state-of-art program FeynHiggs [15, 18-24] to obtain α_{eff} and m_h in the framework of the MSSM.

In Sec. II, we briefly summarize the Higgs precision measurements at various Higgs factories. We also introduce the χ^2 fit formalism used in our analyses. In Sec. III, we discuss the MSSM Higgs sector and stop sector that are needed in our analyses, as well as the SM-like Higgs couplings in the MSSM. In Sec. IV, we summarize the current direct search limits on the mass of the *CP*-odd Higgs and the stop sector. In Sec. V, we perform detailed analyses of various contributions to the total χ^2. In Sec. VI, we present the 95% C.L. allowed region of the MSSM parameter space under the CEPC precisions. In Sec. VII, we compare the reach of the CEPC, the FCC-ee and the ILC. We reserve Sec. VIII for conclusions.

II. HIGGS PRECISION MEASUREMENTS AND χ^2 FIT

Analyses of precision measurements of Higgs decay channels have been performed for the CEPC [3,25], the FCC-ee [26-29], and the ILC [6,30-32] in recent years. A summary of the most up-to-date results on $\Delta(\sigma \times \text{Br})/(\sigma \times \text{Br})$, as well as the total production cross section $\Delta\sigma/\sigma$, can be found in Table 3 in Ref. [33], which will be used in our current study. The dominant production channel at $240-250$ GeV is associated Zh production, with the best measured channel being $h \to b\bar{b}$, given its large decay branching fraction. A precision of about 0.3% can be achieved for this channel. The precisions for $h \to gg$, $WW^*, \tau^+\tau^-$ are about 1%, while $h \to c\bar{c}$ is about 2%−3%. The precisions for $h \to ZZ^*, \gamma\gamma$ are worse, about 5%−7%, given its suppressed decay branching fractions. The sensitivities for the three Higgs factories are very similar. The weak boson fusion (WBF) process $e^+e^- \to \nu\bar{\nu}h$ becomes more important at higher center of mass energy, with a precision of about 0.23% for the $h \to b\bar{b}$ channel at the ILC 500 GeV with 4 ab^{-1} integrated luminosity [6,31].

To analyze the implications of Higgs precision measurements for the MSSM parameter space, we perform a multi-variable χ^2 fit

$$\chi^2_{\text{total}} = \chi^2_{m_h} + \chi^2_\mu = \frac{(m_h^{\text{MSSM}} - m_h^{\text{obs}})^2}{(\Delta m_h)^2}$$
$$+ \sum_{i=f,V..} \frac{(\mu_i^{\text{MSSM}} - \mu_i^{\text{obs}})^2}{(\Delta\mu_i)^2}, \qquad (1)$$

in which $\mu_i^{\text{MSSM}} = (\sigma \times \text{Br}_i)_{\text{MSSM}}/(\sigma \times \text{Br}_i)_{\text{SM}}$ is the signal strength for various Higgs search channels. Here $\chi^2_{m_h}$ and χ^2_μ refer to contributions to the overall χ^2_{total} from the Higgs mass and signal strength measurements, respectively. For $\chi^2_{m_h}$, given the small experimental uncertainties and the relatively large theoretical uncertainties in determining m_h in the MSSM, we set Δm_h to be 3 GeV, taking into account uncertainties coming from higher order radiative corrections [20-23], as well as propagating uncertainties from SM input parameters like m_t. Results with smaller $\Delta m_h = 1$ GeV and 2 GeV are also presented in Sec. VI, to show the impact of possible future improvement in m_h calculation including higher order corrections [34]. For χ^2_μ, $\Delta\mu_i$ is the experimental expected precision in determining the signal strength for a particu-

---

1) For simplicity, we have taken the left and right stop mass parameters to be the same.

lar Higgs decay channel.

For future Higgs factories, $\mu_i^{\rm obs}$ are set to be unity in our analyses, assuming no deviations from the SM predictions are observed. If deviations are observed in the future, we can use the same χ^2 fit method to determine the constrained parameter space, with $\mu_i^{\rm obs}$ being the observed experimental central value [35]. Usually, the correlations among different search channels at Higgs factories are not provided and are thus assumed to be zero.

In our analyses, we determine the allowed parameter region at 95% confidence level (C.L.) by a multi-variable fit to the Higgs decay signal strengths of various channels and Higgs masses. For the one-, two- or three-parameter fit, the corresponding $\Delta\chi^2 = \chi^2 - \chi^2_{\rm min}$ at 95% C.L. is 3.84, 5.99 or 7.82, respectively. Note that when we present the results of our three-parameter fit in Sec. VI, we project the three-dimensional space onto a two-dimensional plane for several benchmark points in the third dimension of the parameter space. Most of the results presented below are for the CEPC precisions. We compare the reaches of the CEPC, the FCC-ee and the ILC in Sec. VII.

III. HIGGS AND STOP SECTOR OF THE MSSM

A. Higgs mass in the MSSM

In our analyses, we identify the light *CP*-even Higgs h in the MSSM as the observed 125 GeV SM-like Higgs. Its mass receives large radiative corrections, dominantly from the stop sector, as well as the sbottom sector at large $\tan\beta$. There have been extensive studies of the MSSM loop correction to the Higgs masses up to next-to-next order [14-16], which includes full one-loop contributions as well as the leading two-loop contributions $O(\alpha_t\alpha_s, \alpha_b\alpha_s, \alpha_t^2, \alpha_t\alpha_b, \alpha_b^2)$ to the Higgs two-point functions. There are also works considering the three-loop effects at order $O(\alpha_{t,b}\alpha_s^2, \alpha_{t,b}^2\alpha_s, \alpha_{t,b}^3)$ [36], as well as approximate evaluation at order $O(\alpha_t^2\alpha_s^2)$ [37].

The *CP*-even Higgs mass matrix is given by

$$\mathcal{M}_{\rm Higgs} = \frac{\sin 2\beta}{2}\begin{pmatrix} \cot\beta\, m_Z^2 + \tan\beta\, m_A^2 & -m_Z^2 - m_A^2 \\ -m_Z^2 - m_A^2 & \tan\beta\, m_Z^2 + \cot\beta\, m_A^2 \end{pmatrix} + \begin{pmatrix} \Delta_{11} & \Delta_{12} \\ \Delta_{12} & \Delta_{22} \end{pmatrix}, \tag{2}$$

with the first term being the tree-level contributions, and $\Delta_{11}, \Delta_{12}, \Delta_{22}$ in the second term being the loop-induced Higgs mass corrections [14,17,38]. The masses for the *CP*-even Higgses are obtained by the diagonalization of the mass matrix:

$$M_{H,h,{\rm eff}}^2 = \frac{m_A^2 + m_Z^2 + \Delta_{22} + \Delta_{11}}{2} \pm \left(\frac{(m_A^2 + m_Z^2)^2 + (\Delta_{22} - \Delta_{11})^2}{4} \right.$$
$$- m_A^2 m_Z^2 \cos^2 2\beta + \frac{(\Delta_{22} - \Delta_{11})\cos 2\beta}{2}(m_A^2 - m_Z^2)$$
$$\left. - \frac{\Delta_{12}\sin 2\beta}{2}(m_A^2 + m_Z^2) + \frac{\Delta_{12}^2}{4} \right)^{1/2}. \tag{3}$$

The effective mixing angle $\alpha_{\rm eff}$ between *CP*-even scalars is defined by

$$\begin{pmatrix} h \\ H \end{pmatrix} = \begin{pmatrix} \cos\alpha_{\rm eff} & \sin\alpha_{\rm eff} \\ -\sin\alpha_{\rm eff} & \cos\alpha_{\rm eff} \end{pmatrix} \begin{pmatrix} {\rm Re}H_u^0 - v_u \\ {\rm Re}H_d^0 - v_d \end{pmatrix}, \tag{4}$$

which takes the form of

$$\tan\alpha_{\rm eff} = \frac{-(m_A^2 + m_Z^2)\sin\beta\cos\beta + \Delta_{12}}{m_Z^2\cos^2\beta + m_A^2\sin^2\beta + \Delta_{11} - m_{h^0,{\rm eff}}^2}. \tag{5}$$

Out of all the supersymmetric particles, the stop sector gives the dominant loop contributions to the Higgs sector. The stop mass matrix depends on the $H_u - H_d$ mixing parameter μ and soft SUSY breaking parameters $m_{\tilde{Q}}$, $m_{\tilde{t}_R}$, and trilinear coupling A_t:

$$\mathcal{M}_{\tilde{t}}^2 = \begin{pmatrix} m_{\tilde{Q}}^2 + m_t^2 + m_Z^2\left(\frac{1}{2} - \frac{2}{3}s_W^2\right)\cos 2\beta & m_t(A_t - \mu\cot\beta) \\ m_t(A_t - \mu\cot\beta) & m_{\tilde{t}_R}^2 + m_t^2 + \frac{2}{3}m_Z^2 s_W^2 \cos 2\beta \end{pmatrix}. \tag{6}$$

The stop left-right mixing parameter is defined as $X_t \equiv A_t - \mu\cot\beta$, which enters the off-diagonal term, and plays an important role in the radiative corrections to the Higgs mass. For our analyses below, we assume mass degeneracy of left- and right-handed top squarks and take the most relevant model parameters as:

$$\tan\beta, m_A, m_{\rm SUSY} \equiv m_{\tilde{Q}} = m_{\tilde{t}_R}, X_t. \tag{7}$$

B. Higgs couplings with $\alpha_{\rm eff}$ method

The effective Lagrangian of the Higgs couplings to a pair of fermions and gauge bosons can be written as [39]

$$\mathcal{L} = \kappa_Z \frac{m_Z^2}{v} Z_\mu Z^\mu h + \kappa_W \frac{2m_W^2}{v} W_\mu^+ W^{\mu-} h + \kappa_g \frac{\alpha_s}{12\pi v} G_{\mu\nu}^a G^{a\mu\nu} h$$
$$+ \kappa_\gamma \frac{\alpha}{2\pi v} A_{\mu\nu} A^{\mu\nu} h - \left(\kappa_t \sum_{f=u,c,t} \frac{m_f}{v} f\bar{f} \right.$$
$$\left. + \kappa_b \sum_{f=d,s,b} \frac{m_f}{v} f\bar{f} + \kappa_\tau \sum_{f=e,\mu,\tau} \frac{m_f}{v} f\bar{f} \right) h \tag{8}$$

with $\kappa_i = g_{hii}^{\mathrm{BSM}}/g_{hii}^{\mathrm{SM}}$ being the Higgs coupling normalized to the SM value. Given that the Yukawa coupling structure of the MSSM is the same as that of the Type-II 2HDM, κ_u, $\kappa_{d,l}$ and κ_V follow the tree-level expression of the Type-II 2HDM, with the mixing angle α being replaced by the effective mixing angle α_{eff} [14,17], including radiative corrections:

$$k_u = \frac{\cos\alpha_{\mathrm{eff}}}{\sin\beta}, \; k_{d,l} = -\frac{\sin\alpha_{\mathrm{eff}}}{\cos\beta}, \; k_V = \sin(\beta - \alpha_{\mathrm{eff}}). \quad (9)$$

This is the so-called "α_{eff} method" [40], which is used in our analyses to count for the MSSM loop corrections to the SM-like Higgs couplings to the SM particles. This effective method is in good agreement with the full loop results [17,41], under the heavy gluino mass assumption that we adopt in our analyses.

Given the high experimental precision in the $h \to b\bar{b}$ channel, $\Delta\mu_b = 0.27\%$ at the CEPC [3,42], and large $\mathrm{Br}_{h\to b\bar{b}} = 57.7\%$, Higgs factories are particularly sensitive to MSSM contributions to κ_b. In addition to the loop contributions to α_{eff}, which enters κ_b via Eq. (9), additional MSSM loop corrections to κ_b are included in our analyses, which is characterized by Δm_b.

$$\kappa_b = -\frac{\sin\alpha_{\mathrm{eff}}}{\cos\beta}\tilde{\kappa}_h^b, \quad \tilde{\kappa}_h^b = \frac{1}{1+\Delta m_b}\left(1 - \Delta m_b \frac{1}{\tan\alpha_{\mathrm{eff}}\tan\beta}\right). \quad (10)$$

Assuming large sbottom and gluino masses, the dominant loop contribution to Δm_b comes from the stop sector [43]:

$$\Delta m_b^{\mathrm{stop}} = \frac{h_t^2}{16\pi^2}\mu A_t \tan\beta I(m_{\tilde{t}_1}, m_{\tilde{t}_2}, \mu). \quad (11)$$

The loop-induced Higgs couplings, hgg and $h\gamma\gamma$ receive contributions from the SUSY sector as well, which are of the same order as the SM contributions. Therefore, hgg and $h\gamma\gamma$ could provide extra sensitivity to the MSSM parameter space [10,12]. In particular, given that the experimental precision for the hgg channel is about 1% at Higgs factories, this channel is particularly sensitive to stops running in the loop. Contributions from the sbottom sector are typically at least an order of magnitude smaller than those from the stop sector, even in the case of large $\tan\beta$ [12]. To focus on the dominant effects, we do not include the sbottom effects in our analyses.

The signal strength μ_i that enters the χ^2 analyses includes the MSSM contributions to both the Higgs production and decays. We use the state-of-art program FeynHiggs [18,20,34,44] to obtain m_h, α_{eff} and Δm_b, calculating the various κs as defined in Eq. (8), which are fed into the evaluation of signal strength μ_i^{MSSM}.

IV. DIRECT SEARCH LIMITS FROM THE LHC

As well as the studies of the SM-like Higgs, there have been extensive searches for MSSM heavy Higgses at the LHC. Given the light *CP*-even Higgs as the observed 125 GeV SM-like Higgs, scenarios such as m_h^{mod} [45], M_h^{125} [46] and hMSSM [47] are proposed to test the model parameter spaces in the $m_A - \tan\beta$ plane. Based on the data collected during the LHC Run 2 with an integrated luminosity of 139 fb^{-1} at $\sqrt{s} = 13$ TeV, the ATLAS collaboration searched for the heavy neutral Higgs bosons over the mass region $0.2-2.5$ TeV with $A/H \to \tau^+\tau^-$ decay [48]. In the M_h^{125} scenario, the data exclude the parameter space of $\tan\beta > 8$ for $m_A = 1.0$ TeV, $\tan\beta > 21$ for $m_A = 1.5$ TeV, and $\tan\beta > 60$ for $m_A = 2.0$ TeV, which are the strongest exclusion limits in the large $\tan\beta$ region. Exclusion from $A/H \to b\bar{b}$ is weaker: for $\tan\beta$ between $20-60$, m_A in the mass region of $0.45-0.9$ TeV has been excluded with bbH/A production in the scenarios of hMSSM [49]. Results from CMS are similar [50].

In the low $\tan\beta$ region, bb and $\tau\tau$ channels are less constraining given the reduced Yukawa couplings. CMS searches with $A/H \to t\bar{t}$ exclude the value of m_A at 400 (700 GeV) for $\tan\beta$ below 1.5 (1.0) [51]. Decay modes of $H \to ZZ$, $A \to hZ$, $H \to WW$, and $H \to hh$ also constrain the parameter space in the low $\tan\beta$ region. Combining the results from these channels, the mass region of $200-600$ GeV is excluded with $\tan\beta$ value between 1 to 6 at both the ATLAS and CMS experiments [52-57]. In addition, CMS searches of $A \to hZ \to \tau\tau\ell\ell$ exclude $\tan\beta$ values below 1.6 at $m_A = 220$ GeV and 3.7 at $m_A = 300$ GeV [58] in the hMSSM scenario.

Searches for charged Higgses produced either in the top quark decay (for $m_H^\pm < m_t$) or associated with a top quark (for $m_H^\pm > m_t$), with the subsequent decay of $H^+ \to \tau\nu$, are performed in the context of hMSSM at the LHC. For a light charged Higgs with $m_{H^\pm} < m_t$, $m_{H^+} \leqslant 160$ GeV is excluded [59]. For a heavy charged Higgs, the region of $\tan\beta = 20-60$ is excluded with $m_{H^\pm}$ from 200 to 1100 GeV [59]. $H^+ \to tb$ decay mode is sensitive to the low $\tan\beta$ region. Value of $\tan\beta = 1.5-0.4$ are excluded in the m_{H^+} range of 200 GeV to 1.5 TeV in the context of m_h^{mod} scenario [60,61].

For the stop sector, the limits are more complicated, given their dependence on the mass spectrum of charginos and neutralinos, as well as the corresponding decay branching fractions. Several channels of the stop decay to the lighter superparticles have been explored. For $\tilde{t}_1 \to t\tilde{\chi}_1^0/bW\tilde{\chi}_1^0/bf f'\tilde{\chi}_1^0$, the latest results show that the stop mass region of $m_{\tilde{t}_1} < 1.2$ TeV is excluded for $\tilde{\chi}_1^0$ mass below about 500 GeV [62,63]. With a light slepton, the $\tilde{t}_1 \to b\tilde{\chi}_1^+ \to b\nu\tilde{\ell} \to b\nu\ell\tilde{\chi}_1^0$ decay channel can exclude masses up to about 1.4 TeV for $\tilde{t}_1$ and 900 GeV for $\tilde{\chi}_1^0$ with $m_{\tilde{\chi}_1^0} < m_{\tilde{\ell}} < m_{\tilde{\chi}_1^\pm}$ [64].

V. CONTRIBUTIONS TO χ^2

In this section, we choose several typical sets of MSSM model parameters to study the various contributions to χ^2_{total}:

$$m_A = 1000/2000 \text{ GeV}, \mu = 500 \text{ GeV}, \tan\beta = 3/30,$$
$$X_t \in (-5000, 5000) \text{ GeV}, m_{\text{SUSY}} \in (200, 3000) \text{ GeV}. \quad (12)$$

To identify the stop contributions, we decouple the masses of other sfermions and gluinos. We scan over the parameter space of X_t and m_{SUSY} to explore the various contributions to the overall χ^2_{total} in Fig. 1, with the colored area being the 95% C.L. allowed region, corresponding to $\Delta\chi^2 = \chi^2 - \chi^2_{\min} = 5.99$ for the two-parameter fit. Different color bands correspond to the χ^2 value. The four columns in Fig. 1 are $\chi^2_{m_h}$ representing the contribution from the Higgs mass, $\chi^2_{gg+\gamma\gamma}$ representing contributions from the loop-induced processes $h \to gg$ and $h \to \gamma\gamma$, $\chi^2_{\mu'}$ representing contributions from tree-level

Higgs decays to SM fermions and vector bosons, and χ^2_{total}, from left to right. The three rows are for $(m_A, \tan\beta) = (1 \text{ TeV}, 30)$, $(2 \text{ TeV}, 30)$ and $(2 \text{ TeV}, 3)$, from top to bottom.

For $m_A = 1$ TeV, $\tan\beta = 30$, $\chi^2_{m_h}$ (top left panel) could push m_{SUSY} to be at least 1.4 TeV with $X_t = 0$, and larger m_{SUSY} is more preferred for such a zero-mixing case. Two max-mixing branches of $|X_t/m_{\text{SUSY}}| \sim 2$ also appear, given that the radiative correction to the Higgs mass is the largest under such a stop maximal mixing region. Larger values of m_{SUSY} are disfavored in these two branches. $\chi^2_{m_h}$ behaviour for $m_A = 2$ TeV, $\tan\beta = 30$ (middle left panel) is very similar to that of $m_A = 1$ TeV, given that the tree-level contributions to m_h are very similar for large m_A at large $\tan\beta$. The lower left panel of $m_A = 2$ TeV, $\tan\beta = 3$, however, shows very different behaviour: the zero mixing region is completely gone and the max-mixing case is preferred with $m_{\text{SUSY}} \gtrsim 1.2$ TeV, given the need for large radiative corrections with the reduced tree-level value of m_h.
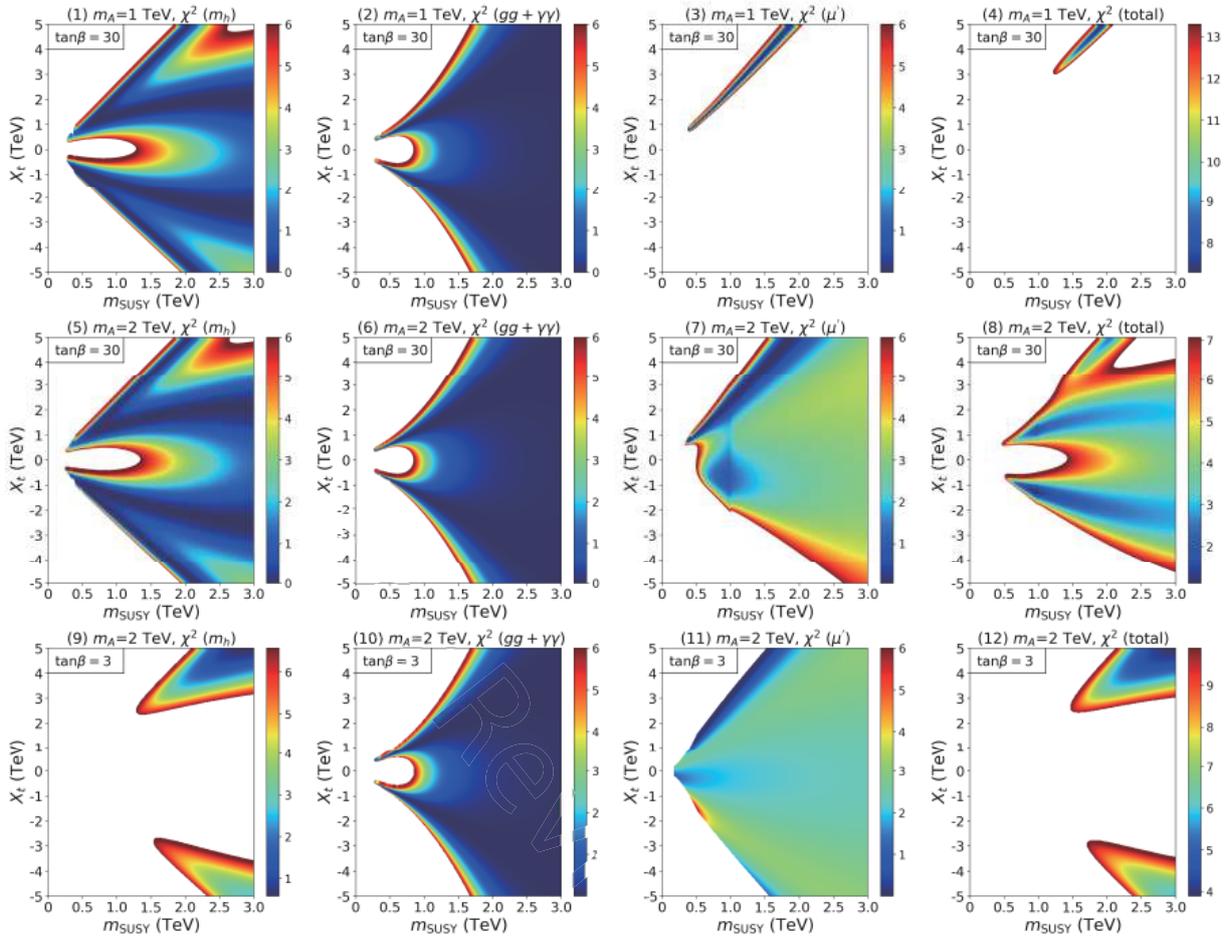
Fig. 1. (color online) 95% C.L. allowed region in the plane of $m_{\text{SUSY}} - X_t$ under CEPC precisions for $(m_A, \tan\beta) = (1 \text{ TeV}, 30)$ (upper panels), $(2 \text{ TeV}, 30)$ (middle panels) and $(2 \text{ TeV}, 3)$ (lower panels). For each row, the panels from left to right show $\chi^2_{m_h}$, $\chi^2_{gg+\gamma\gamma}$, $\chi^2_{\mu'}$, and χ^2_{total}. Different color bands correspond to the χ^2 value. See text for details.

For loop-induced contributions, $\chi^2_{gg+\gamma\gamma}$ (second column), $m_{SUSY} \leqslant 1$ TeV for the zero-mixing case of $X_t = 0$ GeV, as well as $|X_t/m_{SUSY}| > 3$ are excluded, which corresponds to too-large radiative corrections to $h \to gg,\ \gamma\gamma$. There is, however, a large parameter space which remains viable in the m_{SUSY} vs. X_t plane. The dependence of $\chi^2_{gg+\gamma\gamma}$ on m_A and $\tan\beta$ is rather weak.

There are strong constraints coming from the precision measurements of Higgs Yukawa and gauge couplings, as shown in $\chi^2_{\mu'}$ plots in the third column. The most constraining channel is $h \to b\bar{b}$. As a result, for $m_A = 1$ TeV, $\tan\beta = 30$, only the positive branch of X_t survives, as shown in the third panel of the top row. The total χ^2_{total} including all the contributions gives an even more restricted region of $m_{SUSY} \geq 1.2$ TeV and $X_t/m_{SUSY} \sim 2.6$. Sensitivity to κ_b is reduced for larger values of m_A. For $m_A = 2$ TeV, $\tan\beta = 30$, there is a larger allowed parameter region when combining all three χ^2s together. For $m_A = 2$ TeV, with small $\tan\beta = 3$ (bottom row), while the sensitivity to the Higgs precision measurements is similar to that of the large $\tan\beta$ case, stronger constraints from the Higgs mass lead to the final surviving region to be $m_{SUSY} > 1.5$ TeV, $|X_t/m_{SUSY}| \approx 2$ [44].

VI. MULTI-VARIABLE χ^2 FIT RESULTS

In this section, we explore the 95% C.L. allowed region with the Higgs precision measurements at the CEPC in various MSSM parameter spaces. With the four most relevant MSSM parameters (m_A, $\tan\beta$, m_{SUSY}, X_t), we scan in the range:

$$m_A \in (200, 3000)\ \text{GeV}, \tan\beta \in (1, 50),$$
$$X_t \in (-5000, 5000)\ \text{GeV}, m_{SUSY} \in (200, 3000)\ \text{GeV}, \quad (13)$$

with $\mu = 500$ GeV. The fitting results vary little when μ varies. For the 3D fit performed in our analyses, we fix one variable to a set of benchmark values. When presenting results in the 2D parameter space, we project the 3D

results onto the 2D space for a given set of values of the third parameter.

In Fig. 2, we show the 95% C.L. allowed region in the $X_t - m_{SUSY}$ plane for various values of $\tan\beta$ with the CEPC precisions. The left, middle and right panels are for $m_A = 1, 1.5, 2$ TeV, respectively. The low $\tan\beta$ case receives strong constraints from the Higgs mass precision, especially for smaller values of m_A, as explained in the last section. For $m_A = 1$ TeV (left panel), $\tan\beta \leqslant 25$ is completely excluded. The surviving region is around the stop max-mixing section of $|X_t| \approx 2m_{SUSY}$. Only $X_t > 0$ branch survives given the κ^b_h effects, as explained in the last section. For $m_A = 1.5$ TeV (middle panel), $\tan\beta < 10$ is excluded. For $\tan\beta = 10$, a small slice of $X_t < 0$ survives combining all three contributions to χ^2_{total}. Larger regions open up for larger values of $\tan\beta$. For $m_A = 2$ TeV (right panel), $\tan\beta$ as small as 3 is still allowed. Precision constraints from both the mass and the couplings are relaxed for larger $\tan\beta$ and larger m_A, resulting in large survival parameter spaces in X_t vs. m_{SUSY}.

In Fig. 3, we show the 95% C.L. allowed region in the m_{SUSY} vs. m_A plane with the CEPC precisions for $X_t = 0$ (zero-mixing, left panel) and $X_t = 2m_{SUSY}$ (max-mixing, right panel). Regions to the right of the curve are the 95% C.L. allowed regions for different values of $\tan\beta$. For the zero-mixing case, small $\tan\beta$ receives the strongest constraints, with $\tan\beta \leqslant 4$ excluded totally. For the $\tan\beta = 50$, $m_A \geqslant 1350$ GeV and $m_{SUSY} \geqslant 850$ GeV are still allowed. Note that for the zero-mixing case, the most important constraints for m_A come from the Higgs gauge and Yukawa couplings, while the most important constraint for m_{SUSY} comes from the Higgs mass precision, except for the large $\tan\beta$ case, when the Higgs gauge and Yukawa couplings enter as well.

In the max-mixing case, values of $\tan\beta$ as low as 3 could be accommodated. The allowed region is typically larger than that of the zero-mixing case. For small $\tan\beta$, the strongest constraints for m_{SUSY} are the Higgs mass precision and loop-induced hgg and $h\gamma\gamma$. For $\tan\beta \geqslant 7$, the lower limit on m_{SUSY} mostly comes from the loop-in-
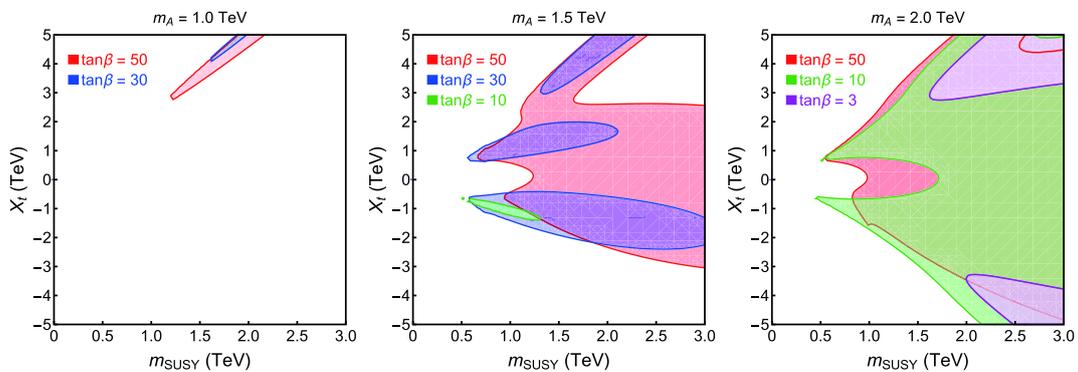
Fig. 2. (color online) 95% C.L. allowed region in X_t vs. m_{SUSY} plane with CEPC precisions for $m_A = 1$ TeV (left panel), 1.5 TeV (middle panel) and 2 TeV (right panel). For each panel, different colored regions correspond to different values of $\tan\beta$.

duced hgg and $h\gamma\gamma$, which are less sensitive to values of $\tan\beta$. There are, however, upper limits on m_{SUSY} from too-large contributions to m_h. Limits on m_A are mostly determined by the precisions of the Higgs couplings.

The results of the three-parameter fit for m_A, m_{SUSY} and $\tan\beta$ are projected onto the m_A vs. $\tan\beta$ plane in Fig. 4. Regions above the curve are the 95% C.L. surviving regions with CEPC precisions for different values of m_{SUSY}. In general, $m_{SUSY} < 900$ GeV is excluded for both the no-mixing and max-mixing cases. For the no-mixing case, when $m_{SUSY} < 1$ TeV, $\tan\beta < 40$ is excluded. Limits on $\tan\beta$ get lower for larger values of m_{SUSY}, which is sensitive in particular for 1 TeV $< m_{SUSY} < 1.5$ TeV. For the max-mixing case, limits on $\tan\beta$ are much lower for $m_{SUSY} = 1$ TeV. Those features are mainly due to the Higgs mass constraint. The LHC Run-II direct search limits based on $A/H \to \tau\tau$ [48] are shown in the grey shaded region, which is complementary to the indirect limits from Higgs precision measurements.

The results of the three-parameter fit for m_A, m_{SUSY} and $\tan\beta$ are projected onto the m_{SUSY} vs. $\tan\beta$ plane in Fig. 5. For each panel, different colored curves correspond to different values of m_A, with the region above the

curve allowed, except for the $m_A = 2$ TeV (blue curves) in the right panel, in which the region between the two curves is allowed. In general, $m_A < 1$ TeV is excluded for both the zero-mixing and max-mixing cases. The lower limits on $\tan\beta$ are relaxed for larger values of m_A, and is sensitive to the values of m_A for 1.5 TeV $< m_A < 2$ TeV. For the max-mixing case and a given m_A, there are upper limits for m_{SUSY} at large $\tan\beta$, as shown in the right panel of Fig. 5. This is due to the too-large contribution to m_h for larger values of m_{SUSY}. For $m_A = 3$ TeV, the upper limit for m_{SUSY} is larger than 3 TeV, and is therefore not shown in the plot.

To illustrate the potential impact of future improvement in the MSSM prediction of m_h, in Fig. 6, we show the 95% C.L. allowed region in m_A vs. m_{SUSY} plane for $\Delta m_h = 3$ GeV (solid curve), 2 GeV (dashed curve), and 1 GeV (dotted curve). The lower limit on m_{SUSY} for the zero-mixing case, and the upper limit on m_{SUSY} for the max-mixing case depend sensitively on the values of Δm_h. Therefore, it is crucial to improve the precision in the m_h calculation in the MSSM, which will allow us to obtain tight constraints on the SUSY mass scale, in particular on the stop sector, once Higgs precision measure-
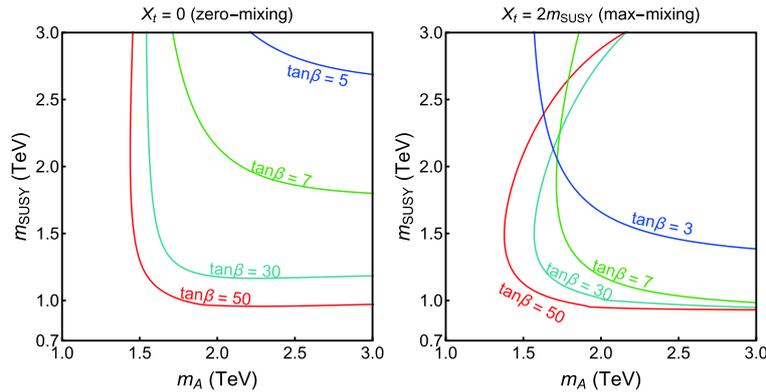
Fig. 3. (color online) 95% C.L. allowed region in the m_{SUSY} vs. m_A plane with CEPC precisions for $X_t = 0$ (zero-mixing, left panel) and $X_t = 2m_{SUSY}$ (max-mixing, right panel). For each panel, different colored curves correspond to different values of $\tan\beta$, with the region to the right of the curve allowed.
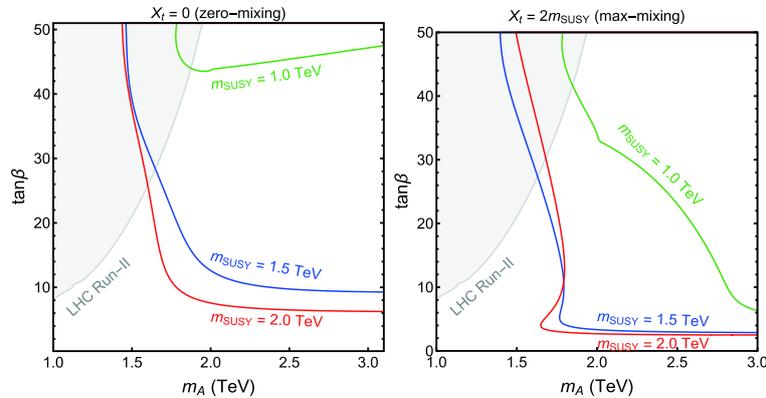
Fig. 4. (color online) 95% C.L. allowed region in the $\tan\beta$ vs. m_A plane with the CEPC precisions for $X_t = 0$ (zero mixing, left panel) and $X_t = 2m_{SUSY}$ (max-mixing, right panel). For each panel, different colored curves correspond to different values of m_{SUSY}, with the region above the curve allowed. The LHC Run-II direct search limits based on $A/H \to \tau\tau$ [48] are shown in the grey shaded region.
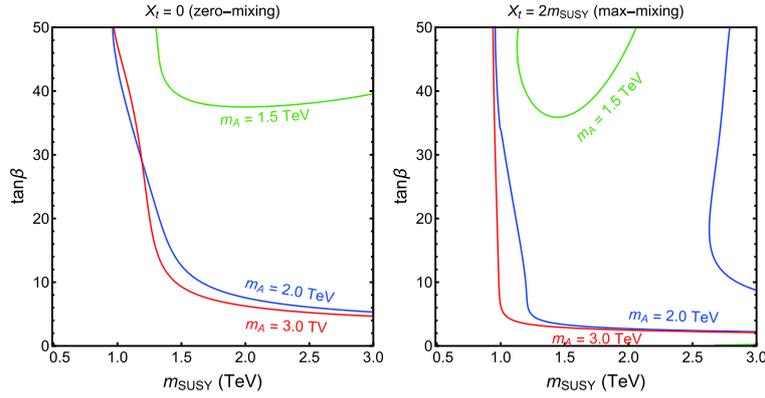
Fig. 5. (color online) 95% C.L. allowed region in the $\tan\beta$ vs. $m_{\rm SUSY}$ plane with the CEPC precisions for $X_t = 0$ (zero-mixing, left panel) and $X_t = 2m_{\rm SUSY}$ (max-mixing, right panel). For each panel, different colored curves correspond to different values of m_A, with the region above the curve allowed, except for $m_A = 2$ TeV (blue curves) in the right panel, in which the region between the two curves is allowed.
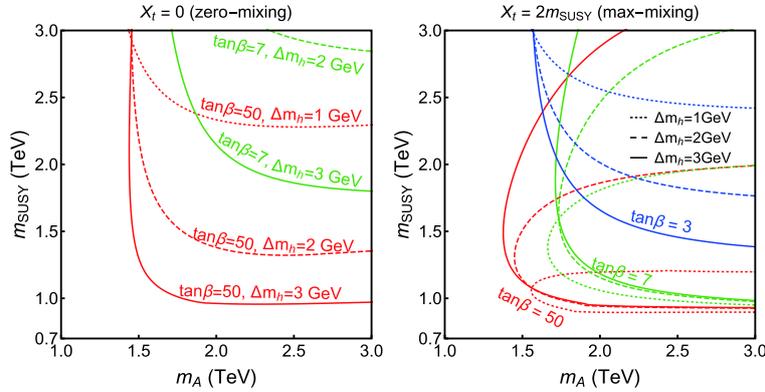
Fig. 6. (color online) 95% C.L. allowed region in the $m_{\rm SUSY}$ vs. m_A plane with CEPC precisions for $X_t = 0$ (zero-mixing, left panel) and $X_t = 2m_{\rm SUSY}$ (max-mixing, right panel). For each panel, different colored curves correspond to different values of $\Delta m_h = 1, 2, 3$ GeV, with the region to the right of the curve allowed.

ments are available at future Higgs factories.

VII. COMPARISON BETWEEN DIFFERENT HIGGS FACTORIES

To compare the reach for three different Higgs factories, we show the 95% C.L. allowed region in [Fig. 7](#) in the parameter space of $m_{\rm SUSY}$ vs. m_A (upper two panels) and $\tan\beta$ vs. m_A (lower two panels) for the zero-mixing and max-mixing cases. While the CEPC and the FCC-ee have similar reach, the reach in m_A for the ILC is better because of better precisions on Higgs measurements of hbb and hWW, given the increased rate of the WBF processes at higher center of mass energies. Limits of $m_{\rm SUSY}$ and $\tan\beta$ (for large $m_{\rm SUSY}$) are nearly the same for all three Higgs factories because they are mainly controlled by the precision in Higgs mass, which comes from theoretical uncertainties. Note that for the m_A vs. $\tan\beta$ plot, the CEPC results are more constraining than the FCC-ee results for $m_{\rm SUSY} = 1$ TeV, while they are nearly the same for $m_{\rm SUSY} = 2$ TeV. This is due to the slightly better precision in $h \to gg, \gamma\gamma$ channel at the CEPC, which makes it

more sensitive for smaller stop mass running in the loop.

VIII. CONCLUSION AND OUTLOOK

In this work, we have studied the constraints of Higgs precision measurements from future Higgs factories on the MSSM parameter space. We considered the dominant stop contributions to the Higgs mass, loop-induced $h\gamma\gamma + hgg$ couplings, and the effective mixing angle $\alpha_{\rm eff}$, which enters the Higgs couplings to a pair of fermions and gauge bosons, as well as additional loop contributions to the bottom Yukawa coupling κ_b. The four relevant parameters under consideration are m_A, $\tan\beta$, $m_{\rm SUSY}$ and X_t.

In the multi-variable χ^2 fit, we included all the Higgs decay channels to SM fermions and gauge bosons at Higgs factories, as well as the Higgs mass. We found that $\chi^2_{m_h}$ dominates for the small $\tan\beta$ case, while χ^2 contributions from the Higgs decays, in particular, $h \to b\bar{b}$, dominates for the small to moderate m_A case. Generally we found that the *CP*-odd Higgs mass m_A is sensitive to the precisions of the Higgs decay channels, while $m_{\rm SUSY}$, X_t
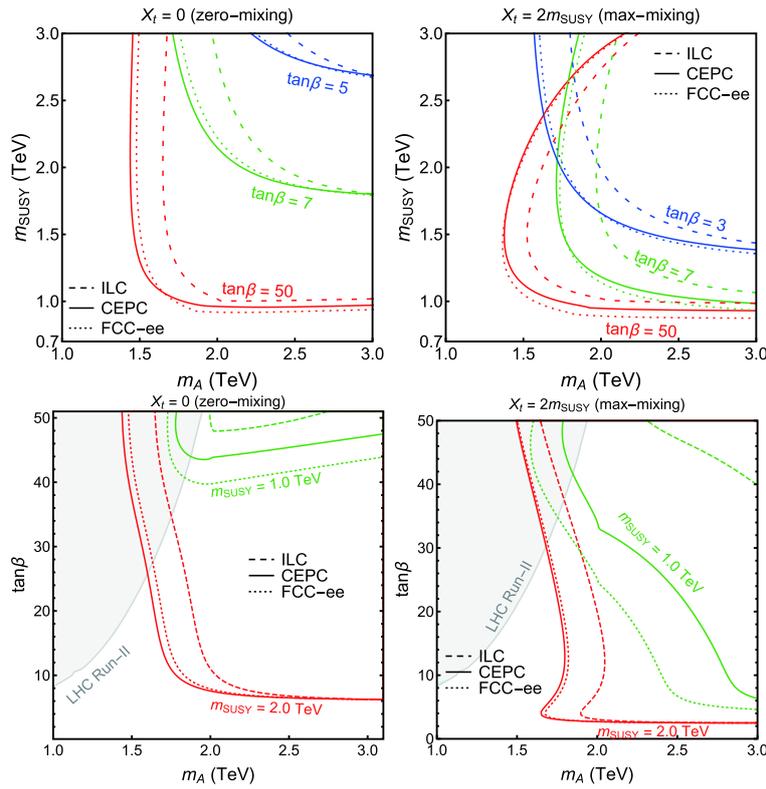
Fig. 7. (color online) 95% C.L. allowed region in the m_{SUSY} vs. m_A plane (top row), and $\tan\beta$ vs. m_A (bottom row) for $X_t = 0$ (zero-mixing, left panels) and $X_t = 2m_{SUSY}$ (max-mixing, right panels), with the CEPC (solid), the FCC-ee (dotted) and the ILC (dashed) precision. The LHC Run-II direct search limits based on $A/H \to \tau\tau$ [48] are shown in the grey shaded region in the bottom panels.

and $\tan\beta$ are sensitive to the precision of Higgs mass determination. For large $\tan\beta$, m_{SUSY} and X_t are also sensitive to the precisions of fermion and vector gauge boson couplings. For the max-mixing scenario, the loop-induced hgg and $h\gamma\gamma$ couplings are the main restrictions on m_{SUSY} when $\tan\beta > 7$.

We obtained the 95% C.L. allowed region given the Higgs factory precisions, and presented the result in the parameter space of M_{SUSY} vs. X_t, M_A vs. m_{SUSY}, m_A vs. $\tan\beta$ and m_{SUSY} vs. $\tan\beta$. We found that small $\tan\beta$ only survives in the max-mixing case with relatively large m_A, while large regions of X_t vs. m_{SUSY} are allowed for large $\tan\beta$ and large m_A. The lower limits on $\tan\beta$ depends sensitively on the values of m_{SUSY} and m_A, in particular, for $m_{SUSY} < 1.5$ TeV and $m_A < 2$ TeV. Limits on m_{SUSY} also depend sensitively on Δm_h, indicating the importance of a precise determination of the Higgs mass in the

MSSM. For $\tan\beta = 50$ of the max-mixing scenario, $m_{SUSY} \in (0.8, 1.2)$ GeV when $\Delta m_h = 1$ GeV.

We also compared the reach of the CEPC, the FCC-ee and the ILC. We found that the reach of the CEPC is similar to that of the FCC-ee, while the reach of the ILC is typically better, given the slightly better precision in the Higgs WBF measurements. With the high precision of the Higgs coupling measurements, and the potential improvement of theoretical calculation of m_h in the MSSM, studying the SM-like Higgs properties at future Higgs factories will offer great insight into the MSSM parameter space, which will be complementary to direct searches for SUSY particles at energy frontier machines.

ACKNOWLEDGMENTS

References

[1] G. Aad *et al.* (ATLAS Collaboration), Phys. Lett. B **716**, 1-29 (2012), arXiv:1207.7214

[2] S. Chatrchyan *et al.* (CMS Collaboration), Phys. Lett. B **716**, 30-61 (2012), arXiv:1207.7235

[3] M. Dong and G. Li (CEPC Study Group Collaboration), *CEPC Conceptual Design Report: Volume 2 - Physics & Detector*, arXiv: 1811.10545

[4] A. Abada *et al.* (FCC Collaboration), *Future Circular Collider: Vol. 1 Physics opportunities*

[5] A. Abada *et al.* (FCC Collaboration), *Future Circular Collider: Vol. 2 The Lepton Collider (FCC-ee)*

[6] P. Bambade *et al.*, *The International Linear Collider: A*

Global Project, arXiv: 1903.01629

[7]   S. Chang, P. J. Fox, and N. Weiner, JHEP **08**, 068 (2006), arXiv:hep-ph/0511250

[8]   S. P. Martin, A Supersymmetry primer **21**, 1-153 (2010), arXiv:hep-ph/9709356

[9]   N. D. Christensen, T. Han, and S. Su, Phys. Rev. D **85**, 115018 (2012), arXiv:1203.3207

[10]   J. Fan, M. Reece, and L.-T. Wang, JHEP **08**, 152 (2015), arXiv:1412.3107

[11]   J. Fan and M. Reece, JHEP **06**, 031 (2014), arXiv:1401.7671

[12]   A. Drozd, J. Ellis, J. Quevillon *et al.*, JHEP **06**, 028 (2015), arXiv:1504.02409

[13]   A. Drozd, J. Ellis, J. Quevillon *et al.*, JHEP **03**, 180 (2016), arXiv:1512.03003

[14]   M. Carena, J. R. Espinosa, M. Quiros *et al.*, Phys. Lett. B **355**, 209-221 (1995), arXiv:hep-ph/9504316

[15]   S. Heinemeyer, W. Hollik, and G. Weiglein, Comput. Phys. Commun. **124**, 76-89 (2000), arXiv:hep-ph/9812320

[16]   M. Carena, S. Heinemeyer, C. Wagner *et al.*, Eur. Phys. J. C **26**, 601-607 (2003), arXiv:hep-ph/0202167

[17]   A. Dabelstein, Nucl. Phys. B **456**, 25-56 (1995), arXiv:hep-ph/9503443

[18]   H. Bahl, T. Hahn, S. Heinemeyer *et al.*, Comput. Phys. Commun. **249**, 107099 (2020), arXiv:1811.09073

[19]   H. Bahl, S. Heinemeyer, W. Hollik *et al.*, Eur. Phys. J. C **78**(1), 57 (2018), arXiv:1706.00346

[20]   H. Bahl and W. Hollik, Eur. Phys. J. C **76**(9), 499 (2016), arXiv:1608.01880

[21]   T. Hahn, S. Heinemeyer, W. Hollik *et al.*, Phys. Rev. Lett. **112**(14), 141801 (2014), arXiv:1312.4937

[22]   M. Frank, T. Hahn, S. Heinemeyer *et al.*, JHEP **02**, 047 (2007), arXiv:hep-ph/0611326

[23]   G. Degrassi, S. Heinemeyer, W. Hollik *et al.*, Eur. Phys. J. C **28**, 133-143 (2003), arXiv:hep-ph/0212020

[24]   S. Heinemeyer, W. Hollik, and G. Weiglein, Eur. Phys. J. C **9**, 343-366 (1999), arXiv:hep-ph/9812472

[25]   CEPC-SPPC Study Group, *CEPC-SPPC Preliminary Conceptual Design Report. 1. Physics and Detector*, http://cepc.ihep.ac.cn/preCDR/volume.html, 2015

[26]   A. Abada *et al.* (FCC Collaboration), Eur. Phys. J. C **79**(6), 474 (2019)

[27]   A. Abada *et al.* (FCC Collaboration), Eur. Phys. J. ST **228**(2), 261-623 (2019)

[28]   M. Bicer *et al.* (TLEP Design Study Working Group Collaboration), JHEP **01**, 164 (2014), arXiv:1308.6176

[29]   N. Alipour Tehrani *et al.*, *FCC-ee: Your Questions Answered, in CERN Council Open Symposium on the Update of European Strategy for Particle Physics* (A. Blondel and P. Janot, eds.), 6, 2019. arXiv: 1906.02693

[30]   H. Baer, T. Barklow, K. Fujii *et al.*, *The International Linear Collider Technical Design Report - Volume 2: Physics*, arXiv: 1306.6352

[31]   K. Fujii *et al.* (LCC Physics Working Group Collaboration), *Tests of the Standard Model at the International Linear Collider*, arXiv: 1908.11299

[32]   K. Fujii *et al.*, *ILC Study Questions for Snowmass 2021*, arXiv: 2007.03650

[33]   N. Chen, T. Han, S. Li *et al.*, *Type-I 2HDM under the Higgs and Electroweak Precision Measurements*, arXiv: 1912.01431

[34]   H. Bahl, S. Heinemeyer, W. Hollik *et al.*, Eur. Phys. J. C **80**(6), 497 (2020), arXiv:1912.04199

[35]   T. Han, S. Li, S. Su *et al.*, *Comparative Studies of 2HDMs under the Higgs Boson Precision Measurements*, arXiv: 2008.05492

[36]   D. Stöckinger and J. Unger, Nucl. Phys. B **935**, 1-16 (2018), arXiv:1804.05619

[37]   R. Harlander, J. Klappert, A. Ochoa Franco *et al.*, Eur. Phys. J. C **78**(10), 874 (2018), arXiv:1807.03509

[38]   R. V. Harlander, J. Klappert, and A. Voigt, *Higgs mass prediction in the MSSM at three-loop level in a pure DR context*, arXiv: 1708.05720

[39]   B. Henning, X. Lu, and H. Murayama, JHEP **01**, 023 (2016), arXiv:1412.1837

[40]   A. Dabelstein, Z. Phys. C **67**, 495-512 (1995), arXiv:hep-ph/9409375

[41]   S. Heinemeyer, W. Hollik, and G. Weiglein, *Decay widths of the neutral CP even MSSM Higgs bosons in the Feynman diagrammatic approach*, hep-ph/0003022

[42]   J. Gu, H. Li, Z. Liu *et al.*, JHEP **12**, 153 (2017), arXiv:1709.06103

[43]   M. Carena, D. Garcia, U. Nierste *et al.*, Nucl. Phys. B **577**, 88-120 (2000), arXiv:hep-ph/9912516

[44]   S. Heinemeyer, Int. J. Mod. Phys. A **21**, 2659-2772 (2006), arXiv:hep-ph/0407244

[45]   M. Carena, S. Heinemeyer, O. Stl *et al.*, Eur. Phys. J. C **73**(9), 2552 (2013), arXiv:1302.7033

[46]   E. Bagnaschi *et al.*, Eur. Phys. J. C **79**(7), 617 (2019), arXiv:1808.07542

[47]   A. Djouadi, L. Maiani, A. Polosa *et al.*, JHEP **06**, 168 (2015), arXiv:1502.05653

[48]   G. Aad *et al.* (ATLAS Collaboration), *Search for heavy Higgs bosons decaying into two tau leptons with the ATLAS detector using pp collisions at √ s = 13 TeV*, arXiv: 2002.12223

[49]   G. Aad *et al.* (ATLAS Collaboration), *Search for heavy neutral Higgs bosons produced in association with b-quarks and decaying to b-quarks at √ s = 13 TeV with the ATLAS detector*, arXiv: 1907.02749

[50]   A. M. Sirunyan *et al.* (CMS Collaboration), JHEP **09**, 007 (2018), arXiv:1803.06553

[51]   CMS Collaboration, *Search for heavy Higgs bosons decaying to a top quark pair in proton-proton collisions at √s = 13 TeV*

[52]   M. Aaboud *et al.* (ATLAS Collaboration), Eur. Phys. J. C **78**(4), 293 (2018), arXiv:1712.06386

[53]   M. Aaboud *et al.* (ATLAS Collaboration), JHEP **03**, 174 (2018), arXiv: 1712.06518, [Erratum: JHEP **11**, 051 (2018)]

[54]   M. Aaboud *et al.* (ATLAS Collaboration), Eur. Phys. J. C **78**(1), 24 (2018), arXiv:1710.01123

[55]   G. Aad *et al.* (ATLAS Collaboration), Phys. Lett. B **800**, 135103 (2020), arXiv:1906.02025

[56]   A. M. Sirunyan *et al.* (CMS Collaboration), JHEP **03**, 034 (2020), arXiv:1912.01594

[57]   A. M. Sirunyan *et al.* (CMS Collaboration), Phys. Lett. B **778**, 101-127 (2018), arXiv:1707.02909

[58]   A. M. Sirunyan *et al.* (CMS Collaboration), JHEP **03**, 065 (2020), arXiv:1910.11634

[59]   M. Aaboud *et al.* (ATLAS Collaboration), JHEP **09**, 139 (2018), arXiv:1807.07915

[60]   A. M. Sirunyan *et al.* (CMS Collaboration), JHEP **01**, 096 (2020), arXiv:1908.09206

[61]   M. Aaboud *et al.* (ATLAS Collaboration), JHEP **11**, 085 (2018), arXiv:1808.03599

[62]   G. Aad *et al.* (ATLAS Collaboration), Eur. Phys. J. C **80**(8), 737 (2020), arXiv:2004.14060

[63]   A. M. Sirunyan *et al.* (CMS Collaboration), JHEP **05**, 032 (2020), arXiv:1912.08887

[64]   A. M. Sirunyan *et al.* (CMS Collaboration), arXiv: 2008.05936